# Dissecting an ancestral neuron network: FIB-SEM-based 3D-reconstruction of the visual neuropils in the sea spider *Achelia langi* (Dohrn, 1881) (Pycnogonida)

Tobias Lehmann[1, 2*], Martin Heß[2, 4], Gerhard Wanner[3], and Roland R. Melzer[1, 2, 4]

**Affiliations**

[1]Bavarian State Collection of Zoology – SNSB, Münchhausenstraße 21, 81247 Munich, Germany

[2]Ludwig-Maximilians-Universität München, Department Biology II, Großhaderner Straße 2, 82152 Planegg-Martinsried, Germany

[3]Ludwig-Maximilians-Universität München, Department Biology I, Großhaderner Straße 2–4, 82152 Planegg-Martinsried, Germany

[4]GeoBio-Center[LMU], Richard-Wagner-Straße 10, 80333 Munich, Germany

[*]Corresponding author: Tobias Lehmann

**Abstract**

**Background:** The research field of connectomics arose just recently with the development of new 3D-EM techniques and increasing computing power. So far, only a few model species (e.g., mouse, the nematode *Caenorhabditis elegans*, and the fruit fly *Drosophila melanogaster*) have been studied using this approach. Here, we present a first attempt to expand this circle to include pycnogonids, which hold a key position for the understanding of arthropod evolution. The visual neuropils in *Achelia langi* are studied using a FIB-SEM crossbeam-workstation, and a 3D serial reconstruction of the connectome is presented.

**Results:** The two eyes of each hemisphere of the sea spider's eye tubercle are connected to a first and a second visual neuropil. The first visual neuropil is subdivided in two hemineuropils, each responsible for one eye and stratified into three layers. Six different neuron types postsynaptic to the retinula axons are characterized by their morphology: five types of descending unipolar neurons and one type of ascending neurons. These cell types are also identified by Golgi impregnations. Mapping of all identifiable chemical synapses indicates that the descending unipolar neurons are postsynaptic to the R-cells and hence are second-order neurons. The ascending neurons are predominantly presynaptic and sometimes postsynaptic to the R-cells and may play a feedback role.

**Conclusions:** Comparing these results with the compound eye visual system of crustaceans and insects – the only arthropod visual system studied so far in such detail – we found striking similarities in the morphology and synaptic organization of the different neuron types. Hence, the visual system of pycnogonids shows features of both median and lateral eyes, which supports the idea that the eyes of pycnogonids are highly ancestral.

**Keywords**

Median eyes, ocelli, lateral eyes, visual system, connectome, Arthropoda, Chelicerata, Pycnogonida

**Background**

One of the most intriguing questions in vision research is how the neuronal circuitry processes the visual input from the photoreceptors, i.e., the neuronal correlate of the eye and retina's visual architecture. Cell-type-specific wiring rules, the divergence and convergence of information channels and the maintenance of retinotopy are some of the core issues. Here, data acquisition entails the challenge of covering volumes of thousands of cubic micrometers (to enclose entire neurons) with a voxel-resolution of only a few nanometers (to correctly trace membrane profiles and to see synaptic structures). One promising approach is (three-dimensional) reconstruction from serial section TEM, which is nowadays a well-established way of analyzing circuitry of neural networks [1], [2], [3]. However, several hundreds of sections or even more have to be cut without any loss of sections, inspected and photographed with the TEM, resulting in an enormous data volume, which is followed by a complex elastic alignment to compensate inevitable image distortions using an elastic alignment program (e.g., TrakEM2 [4], [5]). Hence, the main criterion in selecting a suitable subject for such a study is a small size. In analyzing nervous systems regarding connectomics, either small animals with a small CNS or a restricted region within the CNS or even within a particular neuropil are possible study subjects to obtain a comprehensive data stack.

Early serial section EM research dealing with arthropod visual systems was performed by Macagno et al. [6] in analyzing the visual system in *Daphnia magna* and later by Meinertzhagen and O'Neil [7] in reconstructing synaptic connections in the lamina cartridges of *Drosophila*. A classic example for the reconstruction of a whole nervous system is the nematode *Caenorhabditis elegans* [8], [9]. An early attempt to use computerized 3D reconstructions to study the axonal wiring of photoreceptor axons is that by Melzer et al. [10] in midges and the scorpion fly. These studies did not have today's computing power at their disposal. In the last few years, personal computers have become capable of handling the enormous data volumes inevitable for 3D reconstructions from serial section TEM. Previous studies using this power have focused on the lamina and medulla in the fruit fly *Drosophila melanogaster* [11], [12], [13].

Furthermore, in recent years, a new generation of 3D-EM tools has been developed [14], [15], [16], which includes Serial Block Face Scanning Electron Microscopy (SBF-SEM or simply SBEM) based either on mechanical sectioning [17], [18] or milling with a focused ion beam

(FIB-SEM, [19], [20]). These methods enhanced the potential of 3D-EM considerably and are applied e.g., on nervous tissue [21], [22], [23] and to display and count synapses in vertebrates [24], [25], [26].

In the present study, we analyze the visual neuropils in the pycnogonid *Achelia langi* with one of these methods, namely FIB-SEM. The advantages of this cutting-edge method are that compared to serial section TEM, the generation of the image-stack is much faster and without loss, the images are perfectly aligned with a z-resolution down to 5 nm (TEM approx. 70 nm), and the x-y-resolution and contrast compared to TEM are only slightly reduced.

The Pycnogonida, or sea spiders, are exclusively marine invertebrates, numbering more than 1300 species worldwide [27]. Although largely unnoticed due to their cryptic life habits and economic insignificance, sea spiders are common benthic animals occurring from the littoral zone to the deep sea, from tropical to polar waters. The phylogenetic position of the Pycnogonida has long been controversial and is still under debate. Today, pycnogonids are placed either within the Chelicerata as sister taxon of the Euchelicerata or as sister taxon of all other Euarthropoda [28], [29]. The fossil record indicates that pycnogonids are indeed a highly ancestral group, with the earliest unequivocal records dating back to the Ordovician and Silur [30], [31]. It has even been hypothesized that Pycnogonida might date back to the Cambrian, i.e., the time of the great appendage arthropods [32]. Studies of the cephalon of pycnogonids [33] and of its appendages, e.g., the cheliphores [34], [35], [36] have shown that the innervation pattern of the protocerebrum contributes important sets of characters to the discussion about the phylogenetic position of sea spiders. For this field of research, comparing the structure and development of nervous systems in a phylogenetic context, two different approaches were established: “neurophylogeny” [37], [38] and “neural cladistics” [39].

The sensory parts of the arthropod protocerebrum are primarily responsible for the visual system. Two different types of eyes are found in arthropods, median and lateral eyes. Pycnogonids possess only a periscope-like ocular tubercle with four ocelli generally interpreted as median eyes, whereas classical lateral eyes are absent. Studies using light [40], [41] and electron microscopy [42], [43] have revealed that these eyes are pigment cup ocelli with a cuticular lens and a latticed rhabdom surrounded by pigment layers, features typical of median eyes. Derived conditions might include the structure of the retinula or R-

cells, described as ‘‘pseudoinverted’’ [43], and the presence of a tapetum lucidum (guanine multilayer reflector). The connection of these R-cells to the brain was lately analyzed with classical and modern neuroanatomical techniques to identify the visual neuropils [44]. Hence, the pycnogonid visual system is composed of a thickening dorsolateral to the protocerebrum where the nerve fibers from the two eyes of one hemisphere concentrate, a bifurcated visual tract, and two successive distinct visual neuropils. This innervation pattern is very similar to that in ancestral euarthropods such as the eyes in *Euperipatoides rowelli* (Onychophora) [45] and the median rudimentary eye in *Limulus polyphemus* (Xiphosura) [46], [47].

The architecture of the visual system of sea spiders is relatively simple compared to that of many other arthropods. Considering the phylogenetic position of pycnogonids as an early offspring of the arthropod tree suggested by both tree reconstruction and the fossil record, one can conclude that the selection of Pycnogonida allows us to understand a visual system in a detailed way due to its simplicity and to learn about early eye evolution in arthropods due to its ancestrality.

In the present study, we take a closer look at the visual neuropils in the pyconogonid *Achelia langi* (Ammotheidae) using the advantages of FIB-SEM. In a low-resolution stack, the arrangement of the visual nerve fibers and neuropils is analyzed. In a second, medium-resolution stack, neurons postsynaptic to the R-cells are 3D reconstructed to gain a more detailed view of the neuroanatomy of the pycnogonid visual system. To utilize two strains of evidence, the morphology of these cells is additionally compared to Golgi-impregnated profiles in *Achelia vulgaris*. Finally, in a third high-resolution stack, the distribution of synapses within these cells is analyzed. These findings reveal features of the visual system generally studied in Arthropoda to allow comparisons with other lineages.

## Results

### General layout of the visual neuropils in the protocerebrum

In the examined area of the low-resolution FIB stack, the visual tract bifurcates. After entering the protocerebrum, one part of the fibers projects to the first visual neuropil located dorsolaterally in the anterior part of the protocerebrum as an ovoid region laterally embedded in the cell body rind of the brain (Figs. 1, 2). The other part of the fibers projects

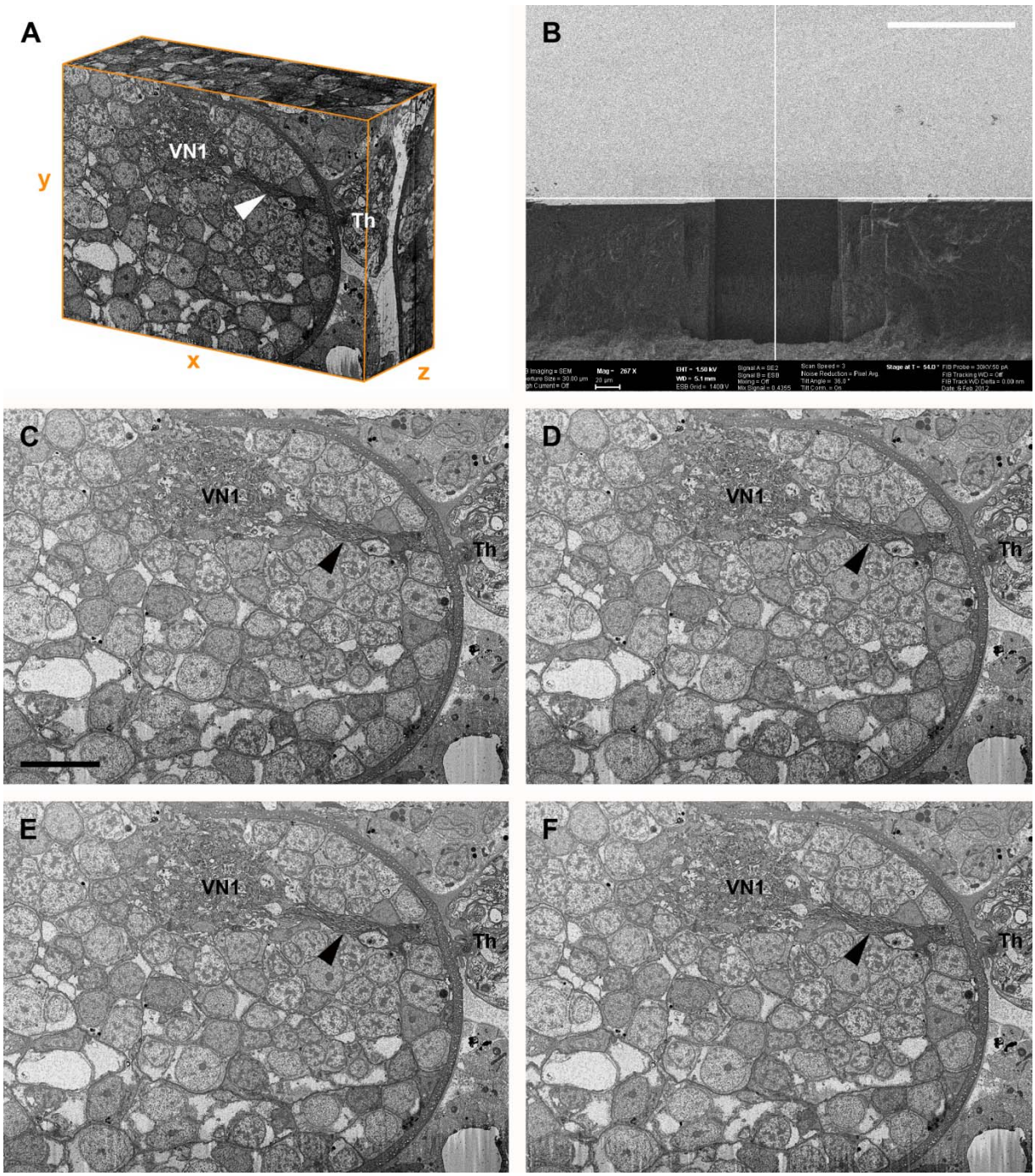


**Figure 1: Pycnogonid visual neuropils studied with focused ion beam SEM technique.**
**A**, 3D volume of low-resolution image stack; note sharp xz- and yz-projections due to almost perfect alignment of FIB-SEM. **B**, backscattered electron image of mesa at beginning of milling by FIB-SEM. Bar 100 µm. **C–F**, short consecutive image series at beginning of stack; note minor but visible structural change from slice no. 80 (C) to slice no. 83 (F). Bar 10 µm.
Arrowhead, visual tract projecting through cell body rind; Th, thickening; VN1, visual neuropil 1.

to the second visual neuropil. These fibers likewise bifurcate and enter the second visual neuropil in two portions. This neuropil is located deeper, under the cell body rind and in a more anterior and central position in the protocerebrum (Fig. 2). Both neuropils are in contact with the rest of the neuropils of the protocerebrum. The posterior part of the first

visual neuropil is ventrally connected to the neuropil of the protocerebrum. The second visual neuropil, in turn, is posteriorly not clearly separated from the remaining neuropils.

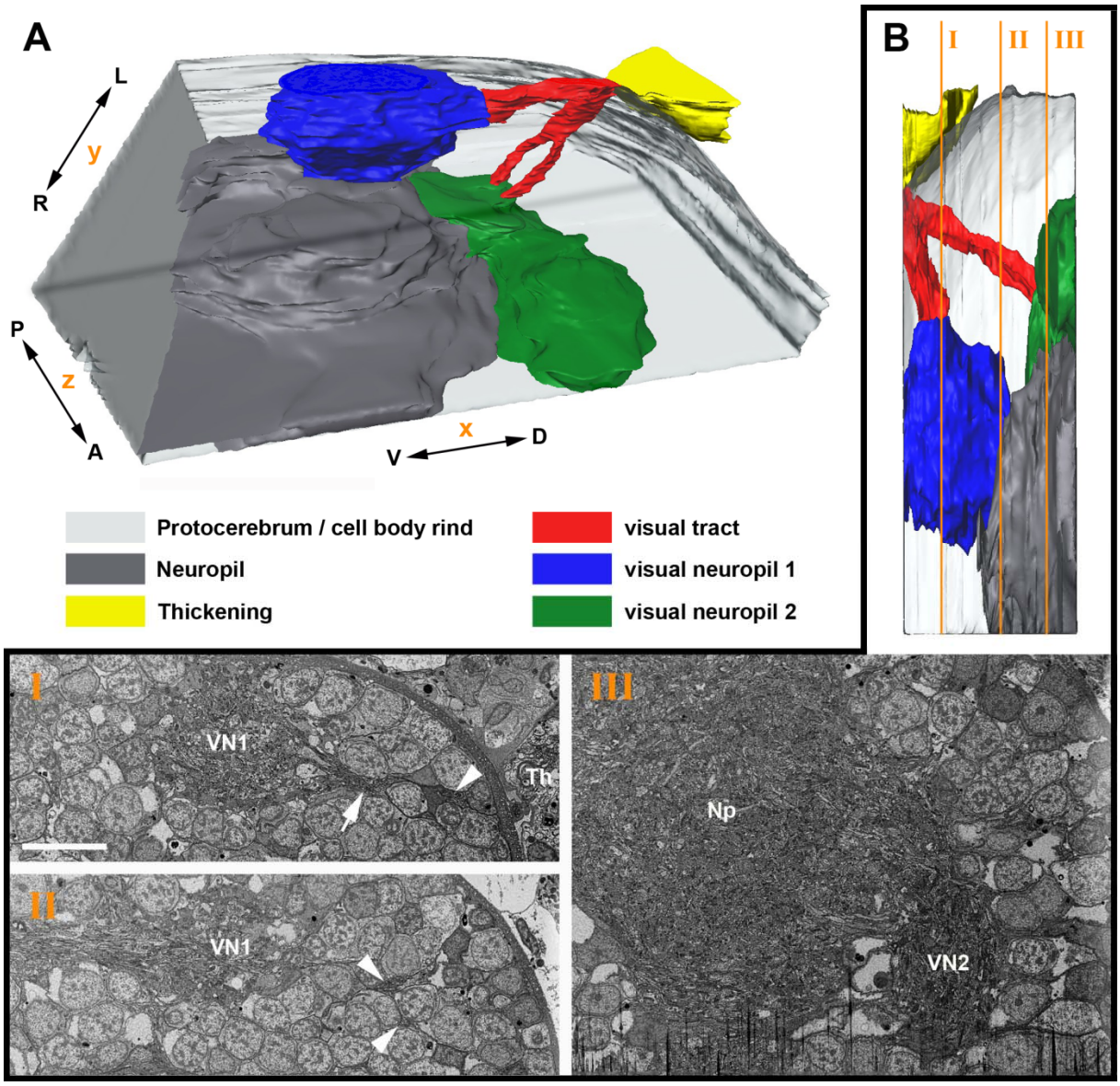


**Figure 2: 3D serial reconstruction of visual neuropils of left hemisphere in *A. langi* on basis of low-resolution image stack.**

**A**, 3D reconstruction showing the arrangement and orientation of neuropils; posterior is up, dorsal is right. **B**, three selected sections showing original data for reconstruction; position of sections indicated in 3D reconstruction top right. **I**, medium range of visual neuropil 1 (slice no. 125); note two subsets of visual tract projecting through cell body rind, arrow indicating subset projecting to visual neuropil 1, arrowhead indicating subset projecting to visual neuropil 2. **II**, low range of visual neuropil 1 (slice no. 376); note two subsets of visual tract projecting through cell body rind to visual neuropil 2 (arrowheads). **III**, beginning of visual neuropil 2 (slice no. 640). Bar 10 µm.

A, anterior; D, Dorsal; L, left; Np, neuropil; P, posterior; R, right; Th, thickening; V, ventral; VN1, visual neuropil 1; VN2, visual neuropil 2.

Cell types in the first visual neuropil

In the FIB-SEM (medium-resolution stack) based examination of *A. langi,* a division of the first visual neuropil into two equal subunits or hemineuropils (see also below) was observed (Figs. 3–6). This division appears in the distal third of the neuropil and is apparent throughout the rest of the neuropil. In the FIB-SEM images, the two hemineuropils are characterized by neurites, mostly of small diameters, and are divided primarily by bulky neurites with larger diameters (Figs. 4B, C).

Furthermore, six different types of neurons were reconstructed and classified on the basis of their morphology: five descending cell types (Figs. 3A–E) and one ascending cell type (Fig. 3F). All of these neurons can also be identified by Golgi impregnations (Fig. 3 rightmost). The descending cells are unipolar neurons with cell bodies in the cell body rind above the neuropil, which send a single neurite each into the first visual neuropil. (To keep the Results section free from homology assumptions, the term 'monopolar cells' is intentionally avoided because this term is occupied by the monopolar cells in the compound eye visual system in Pancrustacea; see discussion). Most of the descending neurons can be traced from the cell body all the way through the neuropil to the end of the image stack. Neurons reconstructed without cell bodies can be allocated to their particular cell type on the basis of the morphology of the neurites. A classification of the ascending neurons cannot be made because the cell bodies of these cells are beyond the examined area. However, the cell bodies must be located below the neuropil, whereas the neurites end before the top end of the neuropil. A large section of the ascending cells and all of the descending cells with cell bodies within the examined volume above the neuropil are reconstructed, and some cells are allocated due to their neurite morphology. Individual retinula axons (cells with a high electron density), due to the low contrast of these cells in the FIB-SEM images, and synapses, due to the too-low resolution, cannot be reliably traced in the medium-resolution stack. In the stack having the highest resolution, however, the R-cells and synapses are reconstructed (see below and Fig. 7). The total volume of interest (i.e., neuropil and cell bodies in the examined area) is approximately 4800 $\mu m^3$, and the volume of all reconstructed cells is 567 $\mu m^3$; hence, the reconstructed cells occupy approximately 12% of the volume.

**Descending unipolar neurons (D1–D5)**

**D1 (Figs. 3A, 4; n=6).** The cell bodies in two of the six cells could be reconstructed; the remaining cells were allocated due to their neurite morphology. Cell bodies are found in the

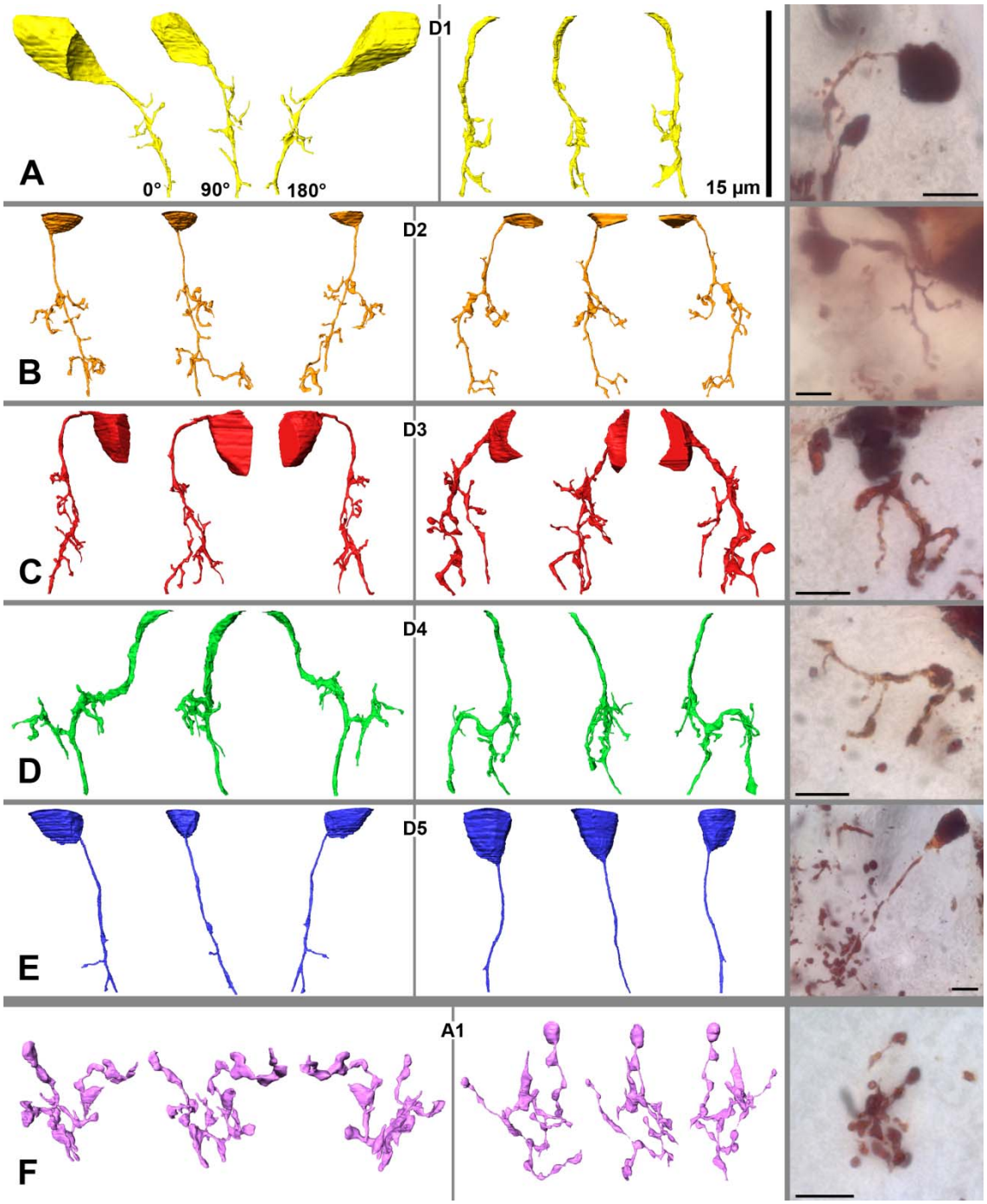


**Figure 3: Profiles of six different cell types found in 3D serial reconstruction of visual neuropil 1 of right hemisphere in *A. langi* on basis of medium-resolution image stack and in Golgi-preparations of *A. vulgaris*.**

Two representatives of each cell type are shown at three different angles; note additional corresponding profiles of Golgi-impregnated cells on right-hand side. **A,** Descending unipolar neuron 1 (D1), characterized by unbranched neurite with several collaterals. **B,** Descending unipolar neuron 2 (D2), characterized by branched neurite with several collaterals. **C,** Descending unipolar neuron 3 (D3), characterized by bifurcation of neurite with several collaterals. **D,** Descending unipolar neuron 4 (D4), characterized by h-shaped neurite with each branch reaching into one hemisphere; with several collaterals as well. **E,** Descending unipolar neuron 5 (D5), characterized by unbranched neurite without or with just few collaterals. **F,** Ascending unipolar neuron 1 (A1), characterized by neurite with multiple branches, each with several large boutons and thin connectors in between. Each cell spreads throughout wide reaches of both hemineuropils.

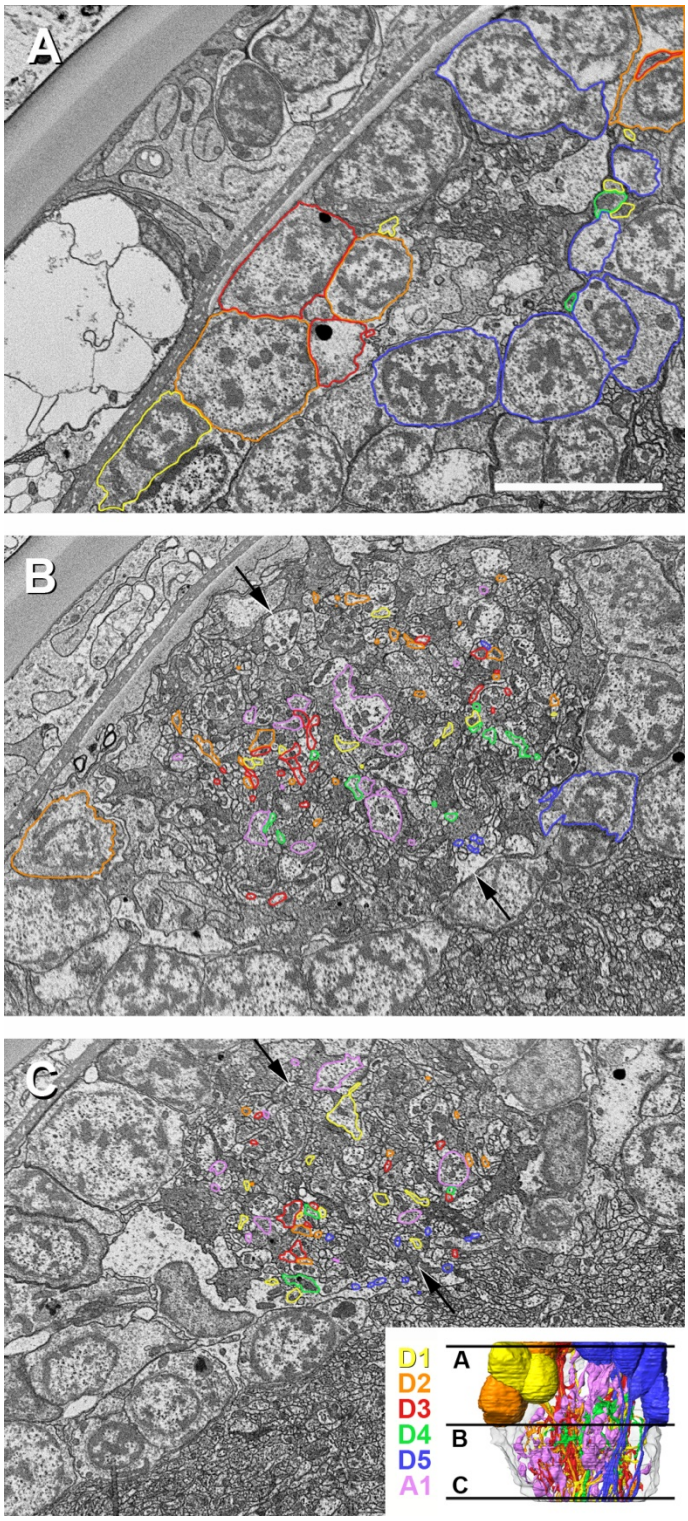


**Figure 4: Three selected sections with labeling of different cell types showing original data for reconstruction.**
Position of sections indicated in 3D reconstruction bottom right; note cells with high electron density identified as retinula axon terminals surrounded by cells with low electron density identified as postsynaptic neurons. **A,** beginning of visual neuropil 1 (slice no. 23); neuropil surrounded by cell bodies of descending unipolar neurons. Bar 5 µm. **B,** medium range of visual neuropil 1 (slice no. 523); arrows indicate subdivision of neuropil into two hemineuropils. **C**, low range of visual neuropil 1 (slice no. 1017); arrows indicate subdivision of neuropil.

cell body rind above or lateral to the upper third of the neuropil. The neurites are unbranched and slightly curved. All cells can be traced to the end of the image stack. Short collaterals occur in tangential and radial directions throughout the neurite but are accumulated in the medium range of the neuropil. Each cell profile covers only a small area of the neuropil. D1 neurons can be found throughout the neuropil, whereas a single neuron is restricted to only one hemineuropil.

**D2 (Figs. 3B, 4; n=5).** The cell bodies could be at least partially reconstructed in all cells. They are found in the cell body rind above or lateral to the upper third of the neuropil. The neurites are branched and slightly curved. The branching always occurs in the medium range of the neuropil, and the neurite is divided into a short and a long branch. The long branch of all cells can be traced to the end of the image stack; the short branch ends in the medium range of the neuropil and is radially oriented. Short collaterals occur in tangential and radial directions throughout both branches of the neurite. Each cell profile covers a larger area of the neuropil compared to the D1 cells. D2 neurons can be found throughout the neuropil, whereas a single neuron is restricted to only one hemineuropil.

**D3 (Figs. 3C, 4; n=6).** The cell bodies could be at least partially reconstructed in four cells; the remaining cells were allocated due to neurite morphology. The cell bodies are found in the cell body rind above or lateral to the upper third of the neuropil. The neurites are bifurcated. The bifurcation always occurs in the medium range of the neuropil. Both branches can be traced to the end of the image stack. Short collaterals occur in tangential and radial directions throughout both branches of the neurite. Similarly to the D2 cells, each cell profile covers a larger area of the neuropil compared to the D1 cells. D3 neurons can be found throughout the neuropil, whereas a single neuron is restricted to only one hemineuropil.

**D4 (Figs. 3D, 4; n=2).** One cell could be reconstructed with only a small portion of the cell body; the other cell was allocated due to the neurite morphology. The cell bodies are found in the cell body rind above the neuropil. The neurites are h-shaped. In the medium range of the neuropil, the neurite is radially oriented and builds two tangential branches, each reaching into one hemineuropil. Short collaterals occur in tangential and radial directions throughout the neurite. All cells can be traced to the end of the image stack. A single D4 neuron occurs in both hemineuropils at once. The cell profiles cover, compared to the other D cells, the largest area of the neuropil because they occur in both hemineuropils.

**D5 (Figs. 3E, 4; n=9).** The cell bodies could be reconstructed at least partially in all cells. They are found in the cell body rind above or lateral to the upper third of the neuropil. The neurites are unbranched, straight or only slightly curved. Six neurons are without any collaterals and three neurons with just one or two short tangential collaterals. All cells can be traced to the end of the image stack. D5 neurons can be found in the right hemineuropil only. These neurons cross the right hemineuropil at its edge, and in the lower part of the neuropil they can be found in the area that divides the two hemineuropils.

**Ascending neurons (A1)**

**A1 (Figs. 3F, 4; n=6).** Cell bodies were not found in the examined area. All reconstructed cells end in the upper third of the neuropil; hence, the neurites could not be traced from the most proximal slice throughout the neuropil to the distal end. The cell bodies of these neurons must therefore be located below the neuropil, meaning that these cells are ascending neurons. The neurites are equipped with multiple branches, each with several large boutons or varicosities and thin connectors in between. These cells have a high-turgor appearance; this means that the boutons have rounded contours. A1 neurons can be found throughout the neuropil; however, branches of A1 neurons accumulate in the area that divides the two hemineuropils. A single neuron occurs in both hemineuropils at once. Each cell profile covers a large area of the neuropil.

Organization of the first visual neuropil

When all neuron types (D1–5, A1) are shown together, no special organization of the neuropil is identifiable (Figs. 5A; 6A). However, by removing the A1 neurons from the 3D reconstruction, a subdivision of the visual neuropil becomes apparent (Figs. 5B; 6B), which is also observed in the FIB-SEM images (see above and Figs. 4B, C). The neuropil is divided into two hemineuropils of equal size. Between the hemineuropils, a border zone exists where less of the D-cells occur. While the D1–4 cells are evenly distributed in both hemineuropils, the D5 cells occur only in the right hemineuropil (Figs. 5B; 6B). When the D5 cells are removed from the reconstruction (Figs. 5C, D; 6C, D) the subdivision becomes more obvious; moreover, a feature of the D4 cell becomes visible: these neurons connect the two hemineuropils. Whereas just a few collaterals of the D1–3 cells reach into the border zone, branches of the D4 cells run through this border and connect both hemineuropils.

When each cell type is shown on its own, their characteristic features become visible (Figs. 5E–J; 6E–J). The D1–3 cells form the main body (apart from the A1 cells) of the visual neuropil (Figs. 5D–G; 6D–G); these cells form the two hemineuropils. Just a few collaterals–but not the main branches–of the D1–3 cells of the two hemineuropil reach into the border zone in between. In contrast to the D1–3 cells, the main branches of the D4 cells cross the border zone and occur in both hemineuropils at once (Figs. 5H; 6H). The D5 cells take a special position; these cells were found in the examined area only in the right hemineuropil (Figs. 5I; 6I). The neurites of the D5 cells run along the posterior edge of this hemineuropil,

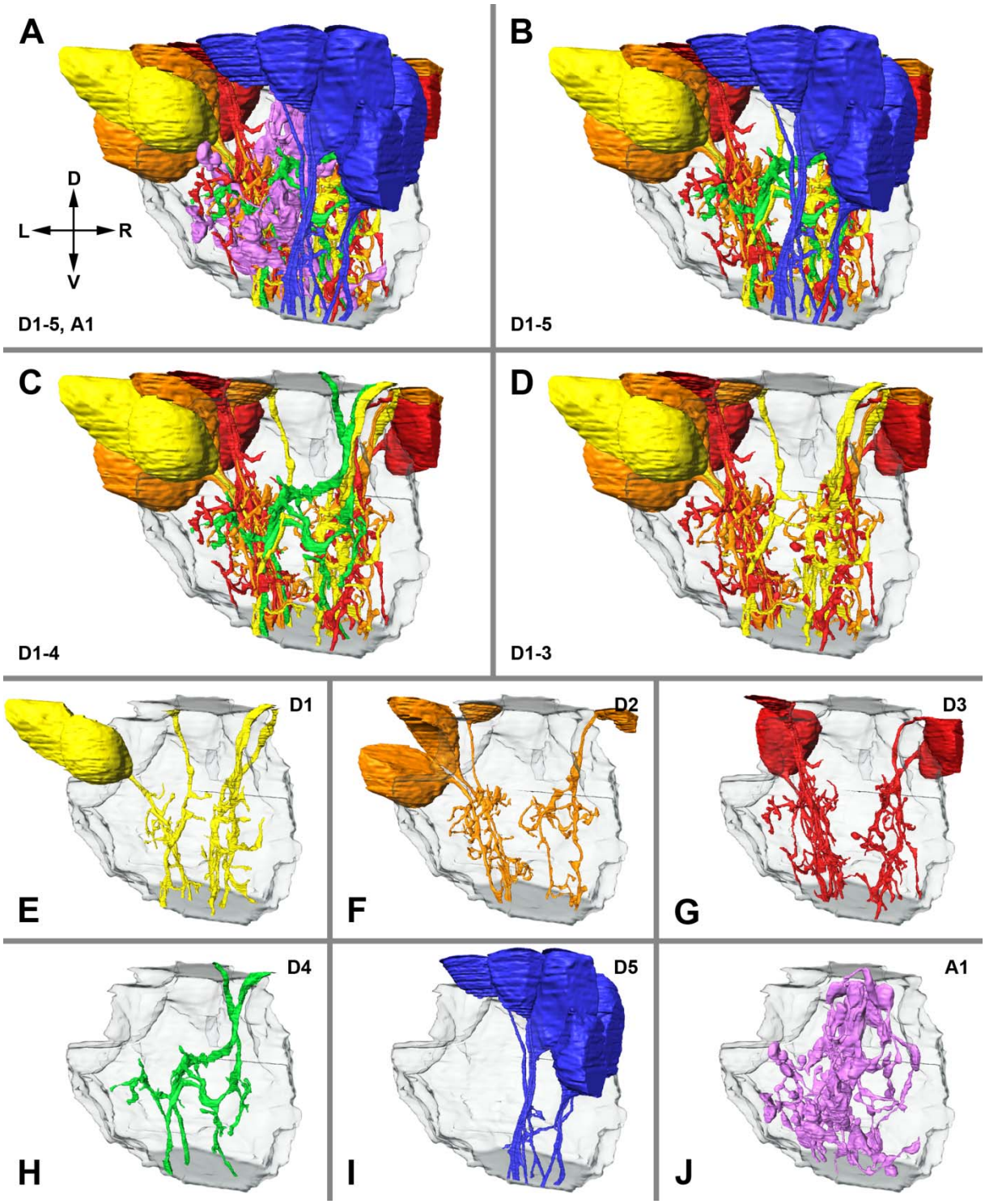


**Figure 5: Lateral view of 3D reconstruction of visual neuropil 1.**
**A**, all reconstructed cells of all six neuron types shown; dorsal is up. **B**, A1 neurons omitted thus subdivision of neuropil gets visible; note D5 neurons mainly in right hemineuropil. **C**, A1 and D5 neurons omitted; note D4 neurons occur in both hemineuropils at once. **D**, A1, D4, and D5 neurons omitted; note D1–3 neurons build two hemineuropils. **E–J**, distribution of different cell types separately within neuropil.
D, dorsal; L, left; R, right; V, ventral.

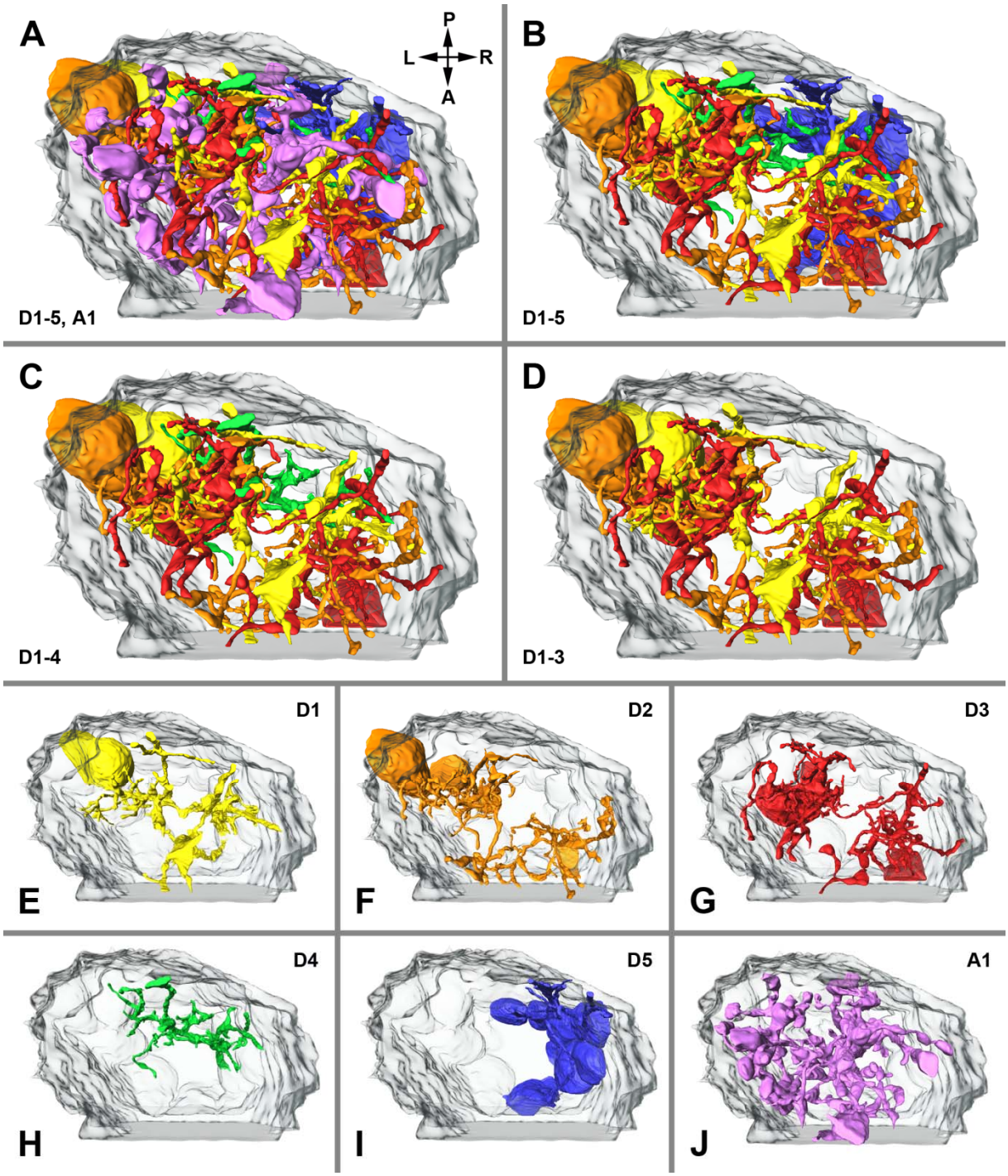


**Figure 6: 3D reconstruction of visual neuropil 1 viewed from bottom up.**
**A**, all reconstructed cells of all six neuron types shown; posterior is up. **B**, A1 neurons omitted thus subdivision of neuropil gets visible; note D5 neurons mainly in right hemineuropil. **C**, A1 and D5 neurons omitted; note D4 neurons occur in both hemineuropils at once. **D**, A1, D4, and D5 neurons omitted; note D1–3 neurons build two hemineuropils. **E–J**, distribution of different cell types within separately neuropil.
A, anterior; L, left; P, posterior; R, right.

and in the lower part they are found primarily in the border zone between the hemineuropils.

The A1 cells can be distinguished from the D1–5 cells in morphology and distribution. These cells do not form two hemineuropils; rather, the neurites of these cells are distributed throughout the neuropil and are accumulated in the border zone of the two hemineuropils.

Synaptic organization of the first visual neuropil

In the stack with the highest resolution, R-cells as well as synapses can be reconstructed in addition to descending and ascending neurons (Fig. 7). The stack is located in the medium range of the neuropil. Cells of one hemineuropil were reconstructed in which three different cell types are allocated on the basis of their neurite morphology: R-cells, D-cells, and A-cells. Ultrastructurally, chemical synapses can be recognized by a presynaptic concentration of electron-dense vesicles and electron-dense material in the synaptic cleft accompanied by high membrane density (Figs. 7F, G). However, postsynaptically, no special synaptic structures are found. In the investigated volume, no sign of electric synapses (e.g., gap junctions) could be detected. Altogether, 95 chemical synapses are identified in the studied volume. These are often multiple-contact synapses (dyads, triads, tetrads, etc.). Altogether, approximately 13% of the cells in the hemineuropil are reconstructed (approximately 260 cells counted in the field of interest in the first slice, 33 cells reconstructed). The total volume of interest (area of the examined hemineuropil) is approximately 260 $\mu m^3$ and the volume of all cells reconstructed is 34 $\mu m^3$; hence, these cells occupy 13% of the volume.

**R-cells (Fig. 7C; n= 18):** This cell type could not be reconstructed in the medium-resolution stack but could in the high-resolution stack. In the FIB-SEM images, these cells are characterized by high electron density. The morphology of R-cells is similar to that of A-cells: the neurites have multiple branches, each with several large boutons or varicosities and thin connectors in between, with the difference that the R-cells have a low-turgor appearance. This means that the shape of these cells adapts to the shape of the surrounding cells and the boutons have limp contours. Within these cells, an average of 3.3 synapses per cell was found in the reconstructed area; these occur primarily in the boutons. R-cells are predominantly presynaptic to D-cells and sometimes to A-cells. Furthermore, R-cells are frequently postsynaptic to A-cells (Tab. 1). One individual R-cell is presynaptic to several D-cells.

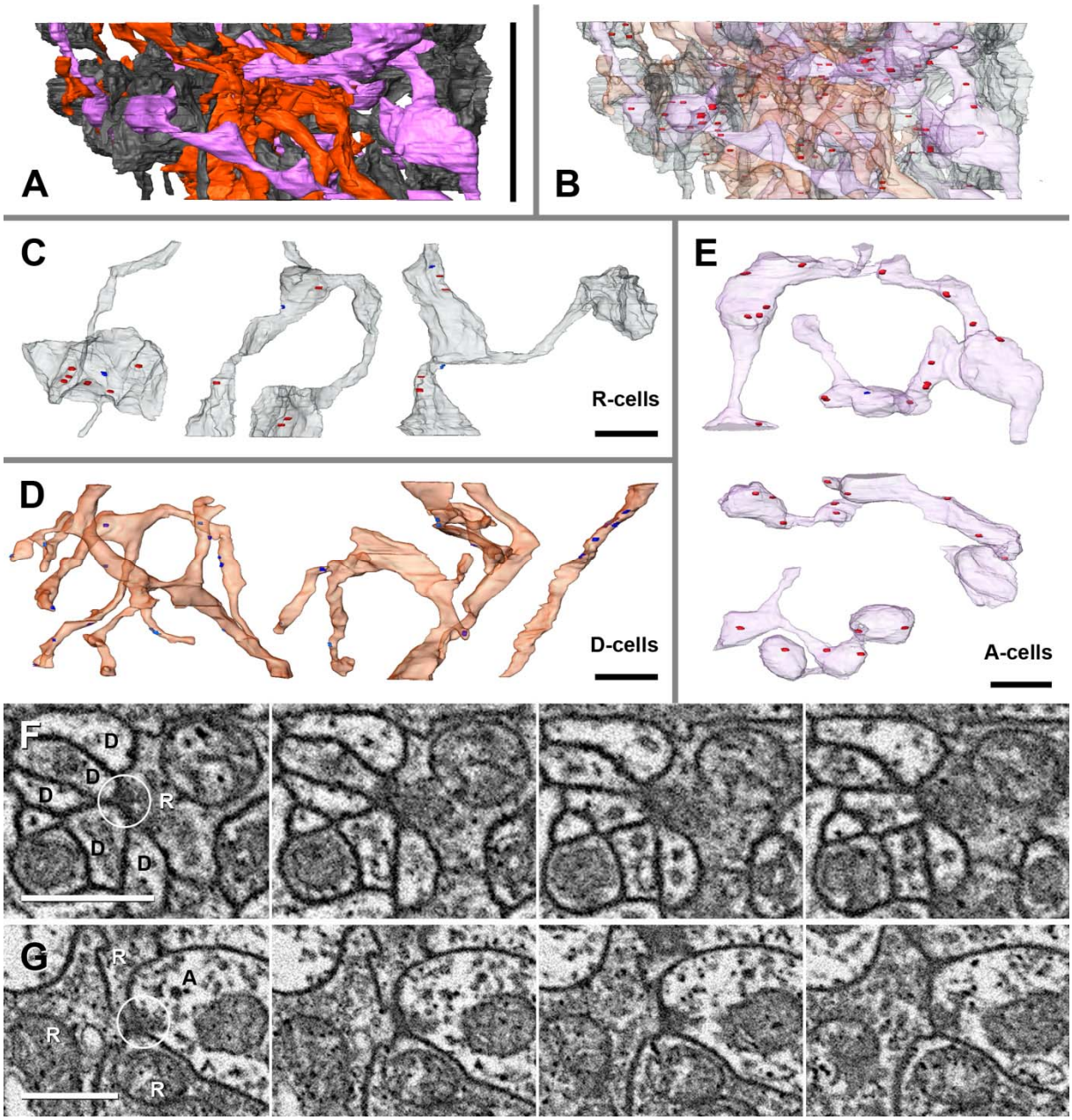


**Figure 7: 3D serial reconstruction of medium range of visual neuropil 1 of right hemisphere in *A. langi* based on high resolution image stack.**

**A,** all reconstructed cells of all three neuron types (R-, D-, and A-cells) shown. Bar 3.2 µm (i.e., z-range of the stack). **B**, all reconstructed cells of all three neuron types (R-, D-, and A-cells) shown in transparent and all chemical synapses (presynaptic vesicle clusters) found within these cells indicated in red. **C**, Profiles of three different R-cells; presynaptic sites indicated in red, postsynaptic sites indicated in blue. Bar 1 µm. **D**, Profiles of three different D-cells; postsynaptic sites indicated in blue, no presynaptic sites in these cells. Bar 1 µm. **E**, Profiles of three different A-cells; presynaptic sites indicated in red, postsynaptic sites indicated in blue. Bar 1 µm. **F**, Series of four consecutive FIB-SEM images showing a synapse (encircled) between R- and D-cells (slice no. 26–29): about five D-cells (cells with low electron density) postsynaptic to one R-cell (cell with high electron density). Bar 500 nm. **G**, Series of four consecutive FIB-SEM images showing a synapse (encircled) between A- and R-cells (slice no. 27–30): three R-cells (cells with high electron density) postsynaptic to one A-cell (cell with low electron density). Bar 500 nm.

**D-cells (Fig. 7D; n=7):** These cells were allocated, due to their neurite morphology, to the D-cells of the medium-resolution stack (Fig. 3). A subdivision into the five different D-cell types cannot be made because only a small portion of the cells on the z-axis were reconstructed. Within these cells, just a few areas with increased vesicle density and other indicators of presynaptic activity were found in the reconstructed area; most cells are without such presynaptic sites. D-cells are predominantly postsynaptic to R-cells and sometimes to A-cells (Tab. 1). One individual D-cell is postsynaptic to several R-cells.

**A-cells (Fig. 7E; n=8):** These cells were allocated, due to their neurite morphology (high-turgor appearance, boutons with connectors), to the A-cells of the medium-resolution stack (Fig. 3). Within these cells, an average of 8.1 synapses per cell is found in the reconstructed area; these are found primarily in the boutons. A-cells are predominantly presynaptic to R-cells and sometimes to D-cells. Furthermore, A-cells are sometimes postsynaptic to R-cells (Tab. 1).

**Table 1: Synaptic pattern of the different cell types in the high-resolution stack.**

| Presynaptic cells | | | → presynaptic to ↓ | |
|---|---|---|---|---|
| R-cells (n=18) | D-Cells (n=7) | A-cells (n=8) | | |
| 0 | 1 | 43 | R-cells | Postsynaptic cells |
| 32 | 1 | 8 | D-cells | |
| 5 | 1 | 0 | A-cells | |
| 22 | 3 | 14 | cells not reconstructed | |
| 3,3 | 0,9 | 8,1 | synapses/cell (average)* | |

* in the reconstructed volume

## Discussion

The term ‘connectome’ refers to the mapping of all neural connections within an organism's nervous system or a confined part of it. These "wiring diagrams" can be defined at different levels of scale, corresponding to levels of interest or the spatial resolution of imaging, for example, the microscale, mesoscale and macroscale [48]. A connectome at the macroscale (light microscope level) attempts to resolve different brain regions or neuropils and the pathways in between; these brain maps were established over the last hundred years for

various species. These days with the help of various new techniques and increased computing power, the meso- and microscale (electron microscope) levels come into focus. At the mesoscale level, the morphology of distinct populations of neurons within a processing unit (e.g., a column or a neuropil) are mapped. This level of analysis can be complemented by the microscale level, which involves mapping single neurons and their connectivity patterns (synapses), which according to Sporns et al. [48] will remain infeasible for an entire brain, at least for the near future. Recently, two ambitious scientific research projects, the Human Brain Project (by the European Union) [49], [50] and the BRAIN Initiative (by the United States) [51], [52], were launched to map these connection patterns in the human brain.

At the meso- and microscale levels, the basic architecture of sensory neuropils in both vertebrates (e.g., the visual cortex in the human brain [53]) and invertebrates (e.g., the optic lobes of the compound eyes in insects and crustaceans [54], [39]) is characterized by columns and layers. The vertical columns, for example, in the insect lamina and medulla [11], [12] are composed of repetitive subsets of afferent fibers (e.g., those of the retinula cells) and characteristic postsynaptic neurons (e.g., monopolar cells) that form the basic functional unit of a system (e.g., visual system). Often, these columns are horizontally layered (e.g., strata M1–6 in the medulla).

In the present study, we analyzed the pycnogonid visual neuropil at macro-, meso- and microscale levels to examine the principles that underlie this (simple) visual system and whether they compare to more complicated ones.

In the low-resolution stack, the macroscale observations of Lehmann et al. [44] can be confirmed. After entering the brain, the fiber bundle with the R-cell axons is split; one part of the axons ends in the first visual neuropil, and the other part passes the first visual neuropil and terminates in the second.

At the mesoscale level, aside from the R-cells, six different cell types can be distinguished in the first visual neuropil: five descending and one ascending cell type. The neuron gestalten are identified with two different approaches, providing support that both our 3D-reconstruction and the Golgi-profiles give correct pictures of the neurons.

Three types of descending cells (D1–3) are responsible for the subdivision of the first visual neuropil into two hemineuropils; these cells do not cross the border in between. In contrast, D4 neurons occur in both hemineuropils at once and provide lateral interactions between

the two hemineuropils. The interpretation of the D5 cells is difficult. Here, these cells are found only in the right hemineuropil, which is most likely a sampling artifact, and the D5-cell bodies of the left hemineuropil are beyond the examined volume and hence are not reconstructed. At the microscale level, the D-cells are frequently postsynaptic to the R-cell axons and hence are second-order neurons. One individual R-cell is presynaptic to several D-cells and one individual D-cell is postsynaptic to several R-cells, indicating divergence and convergence. Concerning the synaptic pattern, no reliable separation between the five different D-cells could be made in the high-resolution stack. However, the reconstructed cells vary in the tangential size of the field they cover in a way that is analogous to their appearance in the medium-resolution stack, indicating that the synaptic pattern is similar in all descending cells.

The ascending neurons are higher-order neurons of a wider field throughout both hemineuropils. These cells are commonly presynaptic and sometimes postsynaptic to R-cells and hence play a feedback role in the system.

Furthermore, at the mesoscale level, it is observed that the first visual neuropil is split into two hemineuropils or columns. This is visible in both the SEM images and the 3D reconstructions. The most plausible explanation of this subdivision is that one hemineuropil is linked to the anterior and the other to the posterior eye of the ocular tubercle. Additionally, in the two hemineuropils, at least three different layers of similar thicknesses are observable. In the upper third of the neuropil, the neurites of the unipolar cells enter the neuropil. Here, just few collaterals were found. In the medium range of the neuropil, a number of things happen: most of the collaterals of the unipolar cells are found here, the branching and bifurcation of the D2 and D3 neurons occurs in this region, and finally the D4 neurons build here their tangential branches that reach into the two hemineuropils. Furthermore, in the medium range of the neuropil, which is analyzed at the microscale level in the high-resolution stack, additionally various synapses occur (whether and where synapses occur in the upper and lower ranges of the neuropil remains unclear at present because these regions were not studied at higher resolution). In the lower third of the neuropil, no more branching or bifurcation occurs, but numerous collaterals are found.

This analysis reveals that the R-cells provide the input into the system, primarily on the D-cells. Because the D-cells rarely appear to be presynaptic in the first visual neuropil, these cells most likely synapse and hence integrate information to higher visual centers that were

not identified in this study. These centers could be the second visual neuropil or the arcuate body, which in chelicerates is closely associated with the visual system [55]. The A-cells play a special role in this system, being pre- and postsynaptic to both R- and D-cells. Hence, these cells collect information from the input (R-cells) and the second-order cells (D-cells) but also circulate information back to these cells. Mechanisms such as lateral inhibition, contrast enhancement, and other filter functions could be behind this feedback loop. Furthermore principles of divergence in the R-cells and convergence in the D-cells are found.

A comparison of our findings with that in other arthropods proves to be difficult, as representatives of only a few taxa have been studied in sufficient detail to allow comparison of neuron morphology. Especially for median eye visual systems, just a few Golgi studies are available.

Hanström [56] reported for *Limulus* that neurites with cell bodies around the neuropil enter the median eye neuropil. Some of these neurites end in the arcuate body and some below the arcuate body. Clear statements on the morphology of these cells are lacking, but their position is the same as the descending unipolar cells found here. Strausfeld et al. [57] reported ascending broad field L-cells in the first median eye neuropil of *Cupiennius salei* (Araneae) that spread through a roughly circular area equivalent to several R-cells. By comparison, the ascending cells of *Achelia langi* also spread through wide reaches of both hemineuropils. Quite revealing is the 3D-EM study by Lacalli [58] of the larval nauplius eye center of the copepod *Dactylopusia sp.* Here, the three eyecups of the nauplius eye are connected to the naupliar eye center. This neuropil is subdivided into three cartridges, each receiving R-cell axons from one of the three eyecups. Several second-order unipolar neurons (LR-cells) with cell bodies above the neuropil postsynaptic to the R-cell axons are found. Additionally, higher-order neurons (M- and E-cells) occur in the neuropil. A similar subdivision (2 ocelli, 2 hemineuropils) is found here in the first visual neuropil of *A. langi*. The morphology and synaptic pattern of copepod LR-cells is similar to that of the pycnogonid D-cells, but cells presynaptic to the R-cells, similar to the A-cells in pycnogonids, have not been identified.

The only arthropod visual system studied in great detail so far is that of the lateral compound eyes in some insect and crustacean species, namely 3D-TEM of *Drosophila* [11], [12], [13], [59], Golgi-studies of insects [60], [61], [39], and Golgi-studies of crustaceans [62], [63], [64], [65]. The lamina's (i.e., first visual neuropil's) cell types are best characterized in

the fruit fly *Drosophila melanogaster*, but the principles are similar in other insect species. The R-cells 1–6 provide input from each ommatidium and synapse to the lamina cartridges, the functional units of the lamina, which are composed of approximately 13 cells: the processes of five monopolar cells (L1–5), one or two amacrine cells, as well as three medulla neurons (C2, C3, and T1) and three glial cells. Additionally, two types of long visual fibers from the ommatidium, R7 and R8, pass the lamina and project to the medulla (second visual neuropil) [7]. In contrast, in crustaceans, R-cells 1–7 end in the lamina and R8 in the medulla. Here also, monopolar cells are found with similar characteristics as in insects. However, there is some disagreement about their number and nomenclature [62], [66], [67].

The synaptic organization in the lamina of *Drosophila* is studied and reviewed in detail by Meinertzhagen and O'Neil [7] and by Meinertzhagen and Sorra [11]. In the lamina, the R-cells are predominantly presynaptic to L1–3 and to amacrine cells. The L-cells in turn have only a few presynaptic sites (to R- and other L-cells) in the lamina. The amacrine cells are frequently presynaptic to R- and L-cells and often to T-cells. Finally, of the medulla neurons, only in C-cells few synapses occur, being presynaptic to L-, T-, and amacrine cells; T-cells are free of synapses in the lamina. All of these synapses are often multiple-contact synapses (dyads, triads, and tetrads).

**Conclusions**

When comparing our results with the characters described in the compound eyes in *Drosophila,* we found striking similarities in the morphology and synaptic pattern of the visual neurons. The situation of the descending unipolar neurons in *Achelia* is similar to the monopolar cells in the compound eyes. Both have their cell bodies above the neuropil, each providing a single neurite that extends through the neuropil. In both, one can distinguish between cells that have collaterals in just one functional unit (i.e., column in *Drosophila* or hemineuropil in *Achelia*; D1–3 in *Achelia* and L1–3 in *Drosophila*) and cells that provide lateral interaction between neighboring columns/hemineuropils (D4 in *Achelia* and L4 in *Drosophila*) and cells without or with very little collaterals in the first visual neuropil that contribute little to the neuropil organization (D5 in *Achelia* and L5 in *Drosophila*). Additionally, the synaptic pattern is similar. The D- and L-cells, respectively, are predominantly postsynaptic to the R-cells, and hence these cells are second-order neurons.

Moreover, in both, these cells are rarely presynaptic to other cells in the particular neuropil. Contrary to these similarities, the morphology of the bifurcated D3 cells in pycnogonids has no counterpart in the compound eye lamina.

Furthermore, the ascending cells that integrate a wider field of the neuropil are found in both systems as well. In *Drosophila* there are three types of ascending cells (amacrine cells and the medulla neurons C and T). In *Achelia,* we found only one not specifically shaped type, but the synaptic pattern of these A-cells resembles the amacrine cells in *Drosophila*. In both species, these cells are frequently presynaptic to R-cells. However, the amacrine cells in *Drosophila* are often also presynaptic to T-cells from the medulla. The medulla has no counterpart in the pycnogonid brain, and hence this cell type and such connections of the ascending neurons are not observed in *Achelia*.

Moreover, the synaptic pattern of the R-cells is the same. In both systems, these cells are predominantly presynaptic to the D- and L-cells, respectively, and frequently to the A- and amacrine cells, respectively, and are postsynaptic to the A- and amacrine cells, again, respectively.

Finally, in both, the synapses between the different cell types are often multiple-contact synapses (dyads, triads, tetrads, or in pycnogonids even more).

Despite this high degree of correspondence, we think it would be premature to use the term homology for the correspondent cell types (D-/L-cells or A-/amacrine-cells) because only a few species have been analyzed at this level.

The pycnogonid visual system stands for a physiologically simple and phylogenetically ancestral one, but we found at least a foreshadowing of the principles of the highly evolved visual systems found in the lateral compound eye of insects and crustaceans. Already, rather than diffusely shaped neurons, distinct neuron types are found that can be characterized by their branching mode, dendrite length, width of the innervated field, and their synaptic pattern. The second-order neurons have a distal cell body and descending neurites that are postsynaptic to terminals of the R-cells. These neurites form functional units (two hemineuropils comparable to the columns in insects and crustaceans), and their branches and collaterals at distinct levels make layers. Additionally, second-order neurons of a wider field are found that connect the hemineuropils, or rather, neighboring columns. And finally, higher-order feedback neurons with ascending neurites and branches that diverge to the wider field of the neuropil, being presynaptic to the R-cells, are found. Additional similarities

with other arthropod median eye neuropils are found in pycnogonids. These are the position of the neuropil and the innervation pattern by the R-cells [44], [68], as well as the subdivision of the neuropil, with each division responsible for one single eye and the presence of unipolar ascending and descending cells.

To put it in a nutshell, the connectome of the first visual neuropil of the pycnogonid *Achelia langi* has a well-organized architecture. It is composed of distinct cell types with characteristic synaptic patterns and already shows principles of the columns and layers design. Additionally, features of both median and lateral eyes are found, which underlines the theory that the eyes of pycnogonids could be older than the appearance of distinct lateral and median eyes.

## Material & Methods

### Specimen collection

Specimens of *Achelia langi* (Dohrn, 1881) (Ammotheidae) were collected for FIB-SEM during field trips in May 2011 to Rovinj (Croatia). Specimens of *Achelia vulgaris* (Costa, 1861) were collected for the Golgi technique during field trips in 2009 and 2010 to Rovinj. Species were determined following Dohrn [69] and Bamber [70].

### FIB/SEM

After dissection of the abdomen, legs, and proboscis in 4% glutardialdehyde in 0.1 M cacodylate buffer at 4°C, the animals were fixed in 4% glutardialdehyde and 1% tannin in 0.1 M cacodylate buffer at 4°C and stored in the fridge at 4°C. After transportation to the lab in Munich, the specimens were osmicated in 1% $OsO_4$ in 0.1 M cacodylate buffer for 2 h at 4°C. To enhance contrast, specimens were en bloc stained with 4% uranyl acetate for 1 h at room temperature. After dehydration in a graded acetone series, the specimens were embedded in epoxy resin (Glycidether 100; 2d at 60°C and 1d at 90°C).

**Low-resolution stack** (transversal view): To approach the visual neuropils, the specimen was trimmed transversally with a diamond knife on an RMC-MTXL ultramicrotome until just before the visual neuropils appeared. After trimming of a cuboid-shaped “mesa” containing the pycnogonid brain with a glass knife [71], this mesa was removed from the epoxy block and mounted on an aluminum stub covered with a thin layer of unpolymerized epoxy resin as glue. The transversal block face was now oriented vertically on the stub, allowing

transversal milling of the left neuropils by the FIB. After polymerizing the epoxy resin (1 d at 60°C), the stub was coated with carbon with a Balzers High Vacuum Evaporator BAE 121 to make it conductive.

The sample was milled and imaged with a Zeiss Auriga CrossBeam Workstation (Carl Zeiss Microscopy, Oberkochen, Germany). For slicing, the conditions were as follows: 500 pA milling current of the Ga-emitter; with each step, 10 nm of the epoxy resin was removed with the focused ion beam. SEM images (2048 x 1536 pixels) were recorded from every 3$^{rd}$ slice at 1.5 kV, resulting in a stack of 682 grayscale images (voxel size 32 x 32 x 30 nm; total volume: 65.5 x 49.2 x 20.5 µm).

**Medium-resolution stack** (frontal view): The specimen was prepared and imaged as for the low-resolution stack, with the only difference being that the specimen was trimmed frontally to allow frontal milling of the left first visual neuropil by the FIB. With a milling rate of 5 nm (every 3$^{rd}$ slice recorded), an image stack with 1031 planes was acquired (voxel size 12 x 12 x 15 nm; total volume: 24.6 x 18.4 x 15.5 µm).

**High-resolution stack** (frontal view): Same specimen as for the medium-resolution stack. The medium range of the contralateral right first visual neuropil was imaged with FIB-SEM with a milling rate of 5 nm (every 3rd slice recorded, 212 images; voxel size 6 x 6 x 15 nm; total volume: 12.3 x 9.2 x 3.2 µm).

Image editing and 3D reconstruction

The images were contrast-enhanced and sharpened using unsharp masking in Adobe Photoshop® CS5 (Adobe Systems), then aligned, manually segmented, and surface rendered in Amira® 5.2.0 (Visualization Sciences Group).

In the medium-resolution stack, the profiles of a representative ensemble of 34 cells were reconstructed. In the high-resolution stack, the profiles of a representative ensemble of 33 cells were reconstructed and presynaptic sites of 95 chemical synapses are localized on the basis of synaptic vesicles. Care was taken that cells postsynaptic to the reconstructed cells were selectively reconstructed as well.

The interactive supplement figure was created following Ruthensteiner and Heß [72] with updated software.

Golgi technique

The abdomen, legs, and proboscis were dissected and the cuticle regions surrounding the central nervous system were perforated to increase the probability of staining the desired

areas. The preparations were submitted to two cycles of the Golgi-Colonnier method [73], embedded in epoxy resin and sectioned (10–20 µm).

## Competing interests

The authors declare that they have no competing interests.

## Authors' contributions

TL and RRM conceived the study. TL and GH performed the experiments. TL and MH analyzed the data. TL, MH, and RRM drafted the manuscript. All authors read and approved the final manuscript.

## Acknowledgements

We thank Silvia Dobler, Heidemarie Gensler, Eva Lodde, and Stefan Friedrich for their expert technical assistance and Hannes Geiselbrecht for his encouraging help with Amira. This study was supported by the Deutsche Forschungsgemeinschaft (DFG Me 2683/6–2).

## References

1. Hoffpauir BK, Pope BA, Spirou GA: **Serial sectioning and electron microscopy of large tissue volumes for 3D analysis and reconstruction: a case study of the calyx of Held**. *Nature protocols* 2007, **2**(1):9-22.
2. Anderson JR, Jones BW, Watt CB, Shaw MV, Yang J-H, DeMill D, Lauritzen JS, Lin Y, Rapp KD, Mastronarde D: **Exploring the retinal connectome**. *Molecular Vision* 2011, **17**:355-379.
3. Bock DD, Lee W-CA, Kerlin AM, Andermann ML, Hood G, Wetzel AW, Yurgenson S, Soucy ER, Kim HS, Reid RC: **Network anatomy and in vivo physiology of visual cortical neurons**. *Nature* 2011, **471**(7337):177-182.
4. Cardona A, Saalfeld S, Preibisch S, Schmid B, Cheng A, Pulokas J, Tomancak P, Hartenstein V: **An integrated micro-and macroarchitectural analysis of the *Drosophila* brain by computer-assisted serial section electron microscopy**. *PLoS biology* 2010, **8**(10):e1000502.
5. Saalfeld S, Fetter R, Cardona A, Tomancak P: **Elastic volume reconstruction from series of ultra-thin microscopy sections**. *Nature Methods* 2012, **9**(7):717-720.
6. Macagno ER, Lopresti V, Levinthal C: **Structure and development of neuronal connections in isogenic organisms: variations and similarities in the optic system of *Daphnia magna***. *Proceedings of the National Academy of Sciences* 1973, **70**(1):57-61.
7. Meinertzhagen IA, O'Neil SD: **Synaptic organization of columnar elements in the lamina of the wild type in *Drosophila melanogaster***. *J Comp Neurol* 1991, **305**(2):232-263.

8. White JG, Southgate E, Thomson JN, Brenner S: **The structure of the nervous system of the nematode *Caenorhabditis elegans***. *Philosophical Transactions of the Royal Society of London B, Biological Sciences* 1986, **314**(1165):1-340.
9. Hall DH, Russell RL: **The posterior nervous system of the nematode *Caenorhabditis elegans*: serial reconstruction of identified neurons and complete pattern of synaptic interactions**. *The Journal of neuroscience* 1991, **11**(1):1-22.
10. Melzer RR, Zimmermann T, Smola U: **Modification of dispersal patterns of branched photoreceptor axons and the evolution of neural superposition**. *Cellular and Molecular Life Sciences CMLS* 1997, **53**(3):242-247.
11. Meinertzhagen IA, Sorra KE: **Synaptic organization in the fly's optic lamina: few cells, many synapses and divergent microcircuits**. *Progress in brain research* 2001, **131**:53-69.
12. Takemura SY, Lu Z, Meinertzhagen IA: **Synaptic circuits of the *Drosophila* optic lobe: the input terminals to the medulla**. *J Comp Neurol* 2008, **509**(5):493-513.
13. Takemura SY, Bharioke A, Lu Z, Nern A, Vitaladevuni S, Rivlin PK, Katz WT, Olbris DJ, Plaza SM, Winston P: **A visual motion detection circuit suggested by *Drosophila* connectomics**. *Nature* 2013, **500**(7461):175-181.
14. Helmstaedter M, Briggman KL, Denk W: **3D structural imaging of the brain with photons and electrons**. *Current opinion in neurobiology* 2008, **18**(6):633-641.
15. Müller-Reichert T, Mancuso J, Lich B, McDonald K: **Three-Dimensional Reconstruction Methods for *Caenorhabditis elegans* Ultrastructure**. *Methods in Cell Biology* 2010, **96**:331-361.
16. Briggman KL, Bock DD: **Volume electron microscopy for neuronal circuit reconstruction**. *Current opinion in neurobiology* 2012, **22**(1):154-161.
17. Denk W, Horstmann H: **Serial block-face scanning electron microscopy to reconstruct three-dimensional tissue nanostructure**. *PLoS biology* 2004, **2**(11):e329.
18. Zankel A, Kraus B, Poelt P, Schaffer M, Ingolic E: **Ultramicrotomy in the ESEM, a versatile method for materials and life sciences**. *Journal of microscopy* 2009, **233**(1):140-148.
19. Gnauck P, Hoffrogge P, Greiser J: **New crossbeam inspection tool combining an ultrahigh-resolution field emission SEM and a high-resolution FIB**. In: *SPIE's 27th Annual International Symposium on Microlithography: 2002*. International Society for Optics and Photonics: 833-840.
20. Principe EL: **How to Use FIB-SEM Data for 3-D Reconstruction**. *R&D Magazine* 2005, **6**:29-30.
21. Briggman KL, Denk W: **Towards neural circuit reconstruction with volume electron microscopy techniques**. *Current opinion in neurobiology* 2006, **16**(5):562-570.
22. Knott G, Marchman H, Wall D, Lich B: **Serial section scanning electron microscopy of adult brain tissue using focused ion beam milling**. *The Journal of neuroscience* 2008, **28**(12):2959-2964.
23. Helmstaedter M, Briggman KL, Denk W: **High-accuracy neurite reconstruction for high-throughput neuroanatomy**. *Nature neuroscience* 2011, **14**(8):1081-1088.
24. Merchan-Perez A, Rodriguez J-R, AlonsoNanclares L, Schertel A, DeFelipe J: **Counting synapses using FIB/SEM microscopy: a true revolution for ultrastructural volume reconstruction**. *Frontiers in neuroanatomy* 2009, **3**:18.
25. Kreshuk A, Straehle CN, Sommer C, Koethe U, Cantoni M, Knott G, Hamprecht FA: **Automated detection and segmentation of synaptic contacts in nearly isotropic serial electron microscopy images**. *Plos One* 2011, **6**(10):e24899.
26. Roncal WG, Kaynig-Fittkau V, Kasthuri N, Berger D, Vogelstein JT, Fernandez LR, Lichtman JW, Vogelstein RJ, Pfister H, Hager GD: **Volumetric Exploitation of Synaptic Information using Context Localization and Evaluation**. *arXiv preprint arXiv:14033724* 2014.
27. Arango CP, Wheeler WC: **Phylogeny of the sea spiders (Arthropoda, Pycnogonida) based on direct optimization of six loci and morphology**. *Cladistics* 2007, **23**(3):255-293.
28. Dunlop JA, Arango CP: **Pycnogonid affinities: a review**. *Journal of Zoological Systematics and Evolutionary Research* 2005, **43**(1):8-21.

29. Regier JC, Shultz JW, Zwick A, Hussey A, Ball B, Wetzer R, Martin JW, Cunningham CW: **Arthropod relationships revealed by phylogenomic analysis of nuclear protein-coding sequences**. *Nature* 2010, **463**(7284):1079-1083.
30. Rudkin DM, Cuggy MB, Young GA, Thompson DP: **An Ordovician Pycnogonid (Sea Spider) with Serially Subdivided 'Head' Region**. *Journal of Paleontology* 2013, **87**(3):395-405.
31. Siveter DJ, Sutton MD, Briggs DE: **A Silurian sea spider**. *Nature* 2004, **431**(7011):978-980.
32. Waloszek D, Dunlop JA: **A larval sea spider (Arthropoda: Pycnogonida) from the Upper Cambrian 'Orsten'of Sweden, and the phylogenetic position of pycnogonids**. *Palaeontology* 2002, **45**(3):421-446.
33. Manuel M, Jager M, Murienne J, Clabaut C, Le Guyader H: **Hox genes in sea spiders (Pycnogonida) and the homology of arthropod head segments**. *Development Genes and Evolution* 2006, **216**(7-8):481-491.
34. Maxmen A, Browne WE, Martindale MQ, Giribet G: **Neuroanatomy of sea spiders implies an appendicular origin of the protocerebral segment**. *Nature* 2005, **437**(7062):1144-1148.
35. Brenneis G, Ungerer P, Scholtz G: **The chelifores of sea spiders (Arthropoda, Pycnogonida) are the appendages of the deutocerebral segment**. *Evol Dev* 2008, **10**(6):717-724.
36. Jager M, Murienne J, Clabaut C, Deutsch J, Le Guyader H, Manuel M: **Homology of arthropod anterior appendages revealed by Hox gene expression in a sea spider**. *Nature* 2006, **441**(7092):506-508.
37. Paul DH: **A neurophylogenist's view of decapod Crustacea.** *Bull Mar Sci* 1989, **45**(2):487-504.
38. Harzsch S: **Neurophylogeny: Architecture of the nervous system and a fresh view on arthropod phyologeny**. *Integr Comp Biol* 2006, **46**(2):162-194.
39. Strausfeld NJ: **Arthropod brains: evolution, functional elegance, and historical significance**. Cambridge, Mass.: Harvard University Press; 2012.
40. Sokolow I: **The structure of the pantopod eyes**. *Z Wiss Zool* 1911, **98**(3):339-380.
41. Helfer H, Schlottke E: **Pantopoda**. Leipzig: Akademische Verlagsgesellschaft m.b.H.; 1935.
42. Jarvis JH, King PE: **Ultrastructure of the Photoreceptors in the Pycnogonid species, *Nymphon gracile* (Leach), and *Pycnogonum littorale* (Strom)**. *Marine and Freshwater Behaviour and Physiology* 1973, **2**:1-13.
43. Heß M, Melzer RR, Smola U: **The eyes of a nobody, *Anoplodactylus petiolatus* (Pantopoda; Anoplodactylidae)**. *Helgol Meeresunters* 1996, **50**(1):25-36.
44. Lehmann T, Heß M, Melzer RR: **Wiring a Periscope – Ocelli, Retinula Axons, Visual Neuropils and the Ancestrality of Sea Spiders**. *Plos One* 2012, **7**(1).
45. Strausfeld NJ, Strausfeld CM, Stowe S, Rowell D, Loesel R: **The organization and evolutionary implications of neuropils and their neurons in the brain of the onychophoran *Euperipatoides rowelli***. *Arthropod Struct Dev* 2006, **35**(3):169-196.
46. Calman BG, Lauerman MA, Andrews AW, Schmidt M, Battelle BA: **Central projections of *Limulus* photoreceptor cells revealed by a photoreceptor-specific monoclonal antibody**. *J Comp Neurol* 1991, **313**(4):553-562.
47. Battelle BA: **The eyes of *Limulus polyphemus* (Xiphosura, Chelicerata) and their afferent and efferent projections**. *Arthropod Struct Dev* 2006, **35**(4):261-274.
48. Sporns O, Tononi G, Kötter R: **The human connectome: a structural description of the human brain**. *PLoS computational biology* 2005, **1**(4):e42.
49. Ailamaki A, Alvandpour A, Amunts K, Andreoni W, Ashburner J, Axer M, Baaden M, Badia R: **The Human Brain Project: A Report to the European Commission**. In. Edited by Markram H. Lausanne: The HBP-PS Consortium; 2012: 107.
50. **Human Brain Project: https://www.humanbrainproject.eu/**
51. Alivisatos AP, Chun M, Church GM, Greenspan RJ, Roukes ML, Yuste R: **The brain activity map project and the challenge of functional connectomics**. *Neuron* 2012, **74**(6):970-974.
52. **BRAIN Initiative: http://www.nih.gov/science/brain/**
53. Bear MF, Connors BW, Paradiso MA: **Neuroscience - Exploring the Brain**, 3rd edn: Lippincott Williams & Wilkins; 2007.

54. Bullock TH, Horridge GA: **Structure and function in the nervous systems of invertebrates**. San Francisco, London: W. H. Freeman and Company; 1965.
55. Homberg U: **Evolution of the central complex in the arthropod brain with respect to the visual system**. *Arthropod Struct Dev* 2008, **37**(5):347-362.
56. Hanström B: **Das Nervensystem und die Sinnesorgane von *Limulus polyphemus*.** *Lunds Universitets Årsskrift* 1926, **22**(5):1-79.
57. Strausfeld NJ, Weltzien P, Barth FG: **Two visual systems in one brain: neuropils serving the principal eyes of the spider *Cupiennius salei***. *J Comp Neurol* 1993, **328**(1):63-75.
58. Lacalli TC: **Serial EM analysis of a copepod larval nervous system: Naupliar eye, optic circuitry, and prospects for full CNS reconstruction**. *Arthropod Struct Dev* 2009, **38**(5):361-375.
59. Sprecher SG, Cardona A, Hartenstein V: **The *Drosophila* larval visual system: High-resolution analysis of a simple visual neuropil**. *Developmental Biology* 2011, **358**(1):33-43.
60. Cajal SR, Sanchez D: **Contribucion al conocimiento de los centros nerviosos de los insectos. Parte I: retina y centros opticos.** *Trabajos del Laboratorio de Investigaciones Biológicas de la Universidad de Madrid* 1915, **13**(1):1-168.
61. Fischbach KF, Dittrich APM: **The optic lobe of *Drosophila melanogaster*. I. A Golgi analysis of wild-type structure**. *Cell and Tissue Research* 1989, **258**(3):441-475.
62. Hafner GS: **The neural organization of the lamina ganglionaris in the crayfish: A Golgi and EM study**. *J Comp Neurol* 1973, **152**(3):255-279.
63. Nässel DR: **The organization of the lamina ganglionaris of the prawn, *Pandalus borealis* (Kröyer)**. *Cell and Tissue Research* 1975, **163**(4):445-464.
64. Stowe S, Ribi WA, Sandeman DC: **The organisation of the lamina ganglionaris of the crabs *Scylla serrata* and *Leptograpsus variegatus***. *Cell and Tissue Research* 1977, **178**(4):517-532.
65. Nässel DR, Elofsson R, Odselius R: **Neuronal connectivity patterns in the compound eyes of *Artemia salina* and *Daphnia magna* (Crustacea: Branchiopoda)**. *Cell and Tissue Research* 1978, **190**(3):435-457.
66. Nässel DR: **Types and arrangements of neurons in the crayfish optic lamina**. *Cell and Tissue Research* 1977, **179**(1):45-75.
67. Sztarker J, Strausfeld NJ, Andrew DR, Tomsic D: **Neural organization of first optic neuropils in the littoral crab *Hemigrapsus oregonensis* and the semiterrestrial species *Chasmagnathus granulatus***. *J Comp Neurol* 2009, **513**(2):129-150.
68. Lehmann T, Melzer RR: **Looking like *Limulus*? – Retinula axons and visual neuropils of the median and lateral eyes of scorpions**. *Frontiers in Zoology* 2013, **10**(1):40.
69. Dohrn A: **Die Pantopoden des Golfes von Neapel und der angrenzenden Meeresabschnitte**. *Monographie der Fauna und Flora des Golfes von Neapel* 1881, **3**:1-252.
70. Bamber RN: **Sea-spiders (Pycnogonida) of the north-east Atlantic: Keys and Notes for Identification the Species**, vol. 5. London, Shrewsbury: Linnean Society of London by Field Studies Council; 2010.
71. Hayat MA: **Principles and techniques of electron microscopy: biological applications**: Cambridge University Press; 2000.
72. Ruthensteiner B, Heß M: **Embedding 3D models of biological specimens in PDF publications**. *Microscopy research and technique* 2008, **71**(11):778-786.
73. Colonnier M: **The Tangential Organization of the Visual Cortex**. *Journal of Anatomy* 1964, **98**:327-344.